5-2023

THE EFFECTS OF RADIATION ON CANCER STEM CELLS IN GLIOBLASTOMA AND OVARIAN CANCER

Aaron Keniston
California State University - San Bernardino

THE EFFECTS OF RADIATION ON CANCER STEM CELLS IN GLIOBLASTOMA AND OVARIAN CANCER

A Thesis

Presented to the

Faculty of

California State University,

San Bernardino

In Partial Fulfillment

of the Requirements for the Degree

Master of Science

in

Biology

by

Aaron Keniston

Graduation Date May 2023

THE EFFECTS OF RADIATION ON CANCER STEM CELLS IN GLIOBLASTOMA AND OVARIAN CANCER

A Thesis

Presented to the

Faculty of

California State University,

San Bernardino

---

by

Aaron Keniston

May 2023

Approved by:

Nicole Bournias-Vardiabasis, Ph.D., Committee Chair, Biology

Juli Unternaehrer, Ph.D., Committee Member

Laura Newcomb, Ph.D., Committee Member

ABSTRACT

High grade serous ovarian cancer (HGSOC) and glioblastoma multiforme (GBM) are some of the most aggressive forms of cancer with poor patient survival. Despite successful cancer therapies, these malignancies have high recurrence rates which can be attributed to cancer stem cells (CSC) due to innate tumor initiating properties. In this study, we investigated the response of CSC populations to proton and photon radiation by quantification of core stem cell transcription factors Sox2 and Oct4. This was carried out utilizing a Sox2/Oct4 green fluorescent protein based reporter designated as SORE6-GFP measured by flow cytometry. We hypothesize that proton and photon irradiation have similar effects of inducing the CSC phenotype measured by SORE6-GFP. Reporter behavior was supported by RT-qPCR, immunofluorescence microscopy and permeabilized flow cytometry data. We found that both proton and photon radiation have similar effects of inducing CSC populations with increasing radiation dosages. Knowing this contributes to developing strategies to combat radiation-induced aggressiveness by targeting CSCs. Inhibiting the action of this cell population can possibly help the prognosis of HGSOC and GBM patients.

ACKNOWLEDGEMENTS

I would first like to thank my committee members Dr. Juli Unternaehrer, Dr. Nicole Bournias-Vardiabasis, and Dr. Laura Newcomb for providing guidance and advice during my masters degree. Dr. Juli Unternaehrer was incredibly supportive of every decision I made during my research at Loma Linda University. Dr Nicole Bournias-Vardiabasis has been an amazing mentor since my undergraduate career and has made this entire experience come to life. Thank you for selecting me as a CIRM graduate student. Dr. Laura Newcomb has also been very involved in my success through my education. I will never forget my first molecular class with you as it was so fun. I would also like to thank my parents for supporting me and pushing me to stay the course. Katie my fiancé has been vital to my success and I would have not made it this for with out her. Last but not least, I would like to thank God for listening to my prayers and staying by my side through the tough times.

TABLE OF CONTENTS

ABSTRACT iii

ACKNOWLEDGEMENTS iv

LIST OF FIGURES vii

CHAPTER ONE: INTRODUCTION 1

Background 1

Ovarian Cancer and Glioblastoma 1

Radiation 2

Effects of Radiation on Cancer Cells 3

Radiation Induced Aggressiveness 4

Cancer Stem Cells 4

Cancer Stem Cell Regulation 6

Cancer Stem Cell Biomarkers 7

CHAPTER TWO: RESULTS 10

Rationale 10

Puromycin Selects for Cells Lenti-virally Transduced 10

Bacterial Transformation of SORE6-GFP Plasmid 11

DNA Digest and Electrophoresis Quality Control Check 13

Cell Panel 15

Immunofluorescence Microscopy Localizes Stemness Transcription Factor Oct4 in the Nucleus of NCCIT Cells 16

Permeabilized Flow Cytometry 18

Gene Expression of Stemness Markers via RT-qPCR 19

SORE6-GFP in Response to Radiation via Flow Cytometry 21

CHAPTER THREE: MATERIALS AND METHODS 25
Cell Culture 25
Bacterial Transformation 26
Miniprep 26
DNA Digest and Gel Electrophoresis 27
Maxiprep 27
293T Transfection for Production of Lentivirus 28
Viral Transduction of Cell Lines and Patient Samples 29
Irradiation 29
Thawing and Cryopreservation 30
Flow Cytometry 30
RT-qPCR 31
Immunofluorescence Microscopy 31
Permeabilized Flow Cytometry 32
CHAPTER FOUR: DISCUSSION 34
REFERENCES 40

LIST OF TABLES

Table 1. Puromycin Concentration to select transduced cell line 11

Table 2. Cell Panel Utilized to Characterize Cancer Stem Cell Response to Radiation 16

Table 3. Quantification of Cell Expressing Oct4 and Sox2 Proteins via Antibody Intracellular Staining 19

LIST OF FIGURES

Figure 1. Schematic of lentiviral stem cell reporter SORE6-GFP 9

Figure 2. Transformed E. coli Plated on LB Agar with Ampicillin 12

Figure 3. SORE6-GFP Plasmid Quality Control Check via Restriction Enzyme Digest and Gel Electrophoresis 15

Figure 4. Immunofluorescence Microscopy Nuclear Localization of Oct4 .. 17

Figure 5. Transcript Analysis of Stemness Markers Sox2, Oct4, and Lin28 in PDX6 20

Figure 6. Selecting for Cancer Stem Cells 21

Figure 7. SORE6-GFP Activity in Response to Proton and Photon Irradiation 24

CHAPTER ONE:

INTRODUCTION

Background

Ovarian Cancer and Glioblastoma

The poor prognosis of ovarian cancer and glioblastoma multiforme (GBM) patients is due to tumor recurrence and metastasis even though first line treatments are successful at reducing tumor burden. More specifically, high grade serous ovarian cancer (HGSOC) is the most common type of ovarian cancer with a 60% mortality rate within 5 years[1], while GBM is the most prevalent and lethal primary brain tumor [2] with a 5 year survival rate of only 6.8%[3]. The first line of defense against HGSOC includes surgical debulking and platinum and taxane based chemotherapies but for GBM radiation is a widely used therapeutic. In recent years, poly (ADP-ribose) polymerase (PARP) inhibitors have also become a mainstay therapeutic against HGSOC and GBM[4]. Inhibition of PARP leads to propagation of single-stranded DNA breaks and accumulation of double-stranded breaks which require homologous recombination repair mechanisms[5]. These treatments do not successfully target all cells that populate tumors which is one reason why GBM and HGSOC have a high recurrence rate.

Emerging evidence shows recurrent tumor cells are more aggressive[1] which is detrimental to these patients because 70% of ovarian cancer patients will relapse within three years[6]. This recurrent aggressiveness is defined by

decreased response to chemotherapy, increased migration, increased invasiveness, or the ability to invade through a basement membrane[7]. In addition, treating ovarian cancer patients with radiation causes high levels of abdominal toxicity, leading to unsatisfactory therapeutic effect in clinical oncology[8]. Being able to modulate cancer aggressiveness will provide insight into ways to provide personalized treatment plans for HGSOC and GBM patients.

Radiation

One way that cancer cells are stimulated to metastasize is by exposure to ionizing radiation (IR)[9,10]. Radiation is included in GBM treatment and causes DNA damage via ROS production[11]. Ovarian cancer is treated with IR in selected cases, usually in cases of advanced disease only, because of the high toxicity level that comes with whole abdomen irradiation. However, because of its potential to mobilize anticancer immunity, radiation therapy is being reconsidered for ovarian cancer[12]. We tested proton and photon irradiation, which have both been utilized for treating a variety of cancers. Some major differences between the two types of radiation are that photon radiation utilizes x-ray beams and deposits high levels of radiation into the surrounded target tissue, while proton radiation uses positively charged particles which results in highly focused tumor radiation deposits. It was shown that exposure to IR increases response to immunotherapy which is another reason to study radiation response in ovarian cancer[10,12]. Ovarian cancers in general are “cold tumors” that harbor a paucity of immune cells, and thus do not respond well to immunotherapy because of the

lack of immune cells infiltrating tumors[13]. During irradiation a “cold tumor” can gain immune cell infiltration therefore being converted to a “hot tumor” with potentially much better response to immunotherapy[14]. A high response to immunotherapy with HGSOC would be of great benefit to patients because healthy cells would remain intact, while cancerous cell would be eliminated.

Effects of Radiation on Cancer Cells

When cancer cells are subject to proton and photon radiation cell death is generally induced through a few different mechanisms. The main objective of radiation is to stop cancer cells from multiplying therefore reducing tumor size and prevent cells left behind from surgical debulking to perpetuate a new tumor. Double stranded DNA breaks are mostly responsible for cell death because as these traumatic events accumulate, the DNA repair mechanisms are not sufficient to maintain cell viability and cell death is induced. Generally, apoptosis and necrosis account for the majority of radiation induced cell death. In addition to double stranded DNA breaks caused directly from radiation, reactive oxygen species (ROS) accumulation is an effect of radiation which is also responsible for DNA damage. ROS production is also associated with mitochondria damage which cascades into apoptotic signaling pathways[15]. Exposure of cancer cells to radiation causes detrimental effects, making radiation a robust clinical approach to combating cancer.

Radiation Induced Aggressiveness

Radiation-induced changes in the tumor microenvironment result in molecular, cellular, and functional changes that can facilitate tumor aggressiveness upon reccurence[16]. This aggressiveness is also due to changes in cancer cell metabolism. One study found that these metabolic alterations promoted GBM progression during recurrence[17]. Since the tumor microenvironment is hypoxic, cancer cells resort to other metabolic pathways such as fatty acid oxidation to produce ATP which is required for respiration and proliferation of cancer cells[18]. Radiotherapy triggers a global adaptive response including increased invasion and migration in glioblastoma cells[19]. When these cells gain these phenotypes it enables them to travel to secondary sites and create metastatic tumors resulting in organ failure and death. Further, cancer stem cell populations can grow after radiotherapy[20] which indicates that cancer stem cells are top priority when considering how to combat post radiation aggressiveness. To expand on this, there is growing literature that shows radiation enriches the CSC population in a variety of cancers[21] including GBM[22] and that transcription factor SOX2[23] is partially responsible for this increase in stemness.

Cancer Stem Cells

Cancer stem cells (CSCs) have been shown to participate in cancer recurrence[24]. Cancer stem cells represent a small subpopulation within a tumor that can self-renew (give rise to more CSCs) and differentiate, which gives rise to

a heterogenous population of cells necessary for tumor survival. CSCs are important for the success of tumors. The CSC concept is not new, but major efforts are needed to better understand CSC physiology. There are several genetic models of how CSCs are generated. One theory is that CSCs arise from normal stem/progenitor cells which acquire the ability to generate tumors due to a genetic mutation[25]. Some CSCs may escape DNA damaging chemotherapies which target the cell cycle because these cells are mitotically quiescent. CSC dormancy is broadly defined as a stalled phase of cell cycle progression during which single cancer cells remain in G0, yet retain the ability to progress into overt disease[26] once signaled to become mitotically active again. This phase may coincide with the tumor being clinically undetectable. It is known that mono-chemotherapy using cytotoxic drugs such as camptothecin (CPT), doxorubicin, and paclitaxel not only cannot kill the highly resistant and mitotically quiescent CSCs, but also increases their ‘stemness’-related properties[27]. Self-renewal properties of CSCs make them targets that cause cancer recurrence. One CSC can give rise to an entire population of CSCs. Another reason why CSCs are thought to drive cancer recurrence is because they can differentiate into all of the cells necessary for tumor survival. One study has shown that in glioblastoma CSCs drive neoangiogenesis[28] which helps bring blood and nutrients to feed the tumor[29]. If CSCs are not eliminated during the course of treatment, cancer recurrence probability is high.

Cancer Stem Cell Regulation

During therapeutic development, CSC regulation has provided substantive breakthroughs for inhibiting cancer growth. The tumor microenvironment provides suitable space for self-renewal and differentiation of CSCs and increases their chemical and radiological tolerance[30] through various signaling pathways such a Notch and Wnt. One study of the vascular niche microenvironment made of primarily epithelial cells showed direct contact between epithelial cells and CSCs in brain tumors causing de-differention events[31] of the epithelial cells. It has been described that the vascular microenvironment maintains the initial dedifferentiation dormancy of stem cells, supports self-renewal, invasion and metastasis of CSCs, and protects them from injury[32].

The immune system has also been characterized to regulate CSCs. In fact, tumor associated macrophages induce cancer cells that express CD133 and Sox2 to reprogram into CSCs through the secretion of mucin-1[33]. Metabolism is yet another hallmark that integrates into CSC regulation. One study showed that IMP2 controls oxidative phosphorylation in primary glioblastoma sphere cultures causing CSC expansion[34]. However, a study using patient derived xenografts expressing CD44 and CD117 were oxidative phosphorylation dependent[35] which suggests that different cancers have a wide variety of biomolecules that regulate CSC metabolism making CSCs hard to target.

Cancer Stem Cell Biomarkers

Previous studies have identified CSC populations using many different biomarkers which has helped the understanding of CSC biology. This pioneering work has made large advances in characterizing the behavior of CSCs but has faced challenges because CSCs have differential biomarker expression between cancer types. For example, CD133 is a surface protein that is expressed on CSCs in hematopoietic and a variety of solid tumors including but not limited to neural[36,37], prostate, colonic, endometrial[38], and ovarian[39–43]. Other attempts to identify CSC populations have included the use of flow cytometry analysis for surface markers CD44 and ALDH. It has been revealed that probing for surface proteins to identify CSCs can be a challenging strategy because these proteins are heterogeneously expressed and the technique requires expensive antibodies. Stemness in a population of cancer cells can also be detected by RT-qPCR. For example, core stem cell transcription factors SOX2 and OCT4 have provided identification of CSC populations[44]. However, this technique is also expensive, time consuming, it is a relative measure of gene expression, and it does not directly measure protein but rather RNA expression. Another downside of the RT-qPCR approach is information of gene expression on an individual cell basis is lost due to whole population mRNA collection.

An alternative modality of characterizing CSC genotypes is via a reporter system. Common reporter systems utilize a fluorescent protein to indicate when specific genes are expressed which can give insight into dynamic cellular

programing of in vitro and in vivo models. When a fluorescent gene is fused to the promotor region of a gene of interest this allows for the fluorescent gene to become expressed in the same manner as the gene of interest being, including being up regulated by transcription factors. CSC populations can be detected with the use of a reporter system designated as SORE6-GFP where the SOX2 and OCT4 response element drives transcription of the green fluorescence protein (GFP) gene (Fig.1)[45]. These CSC populations can then be quantified via flow cytometry. This modality of CSC detection is beneficial because it doesn't require time consuming RT-qPCR experiments or the use of expensive antibodies and can track real time changes in CSC populations. A common challenge with using reporter systems is the sensitivity of the promoter region which regulates the reporter gene. Another downside is that GFP is a transient molecule that can easily be degraded. Getting the reporter system into the cell is also challenging because cells have systems to combat viral transduction. A difficulty of using a reporter is not knowing how many molecules are needed to upregulate GFP enough to create a detectable signal. In addition, reporter systems give a snapshot in time of gene expression levels, which is an everchanging dynamic process. Utilizing a destabilized GFP has its benefits but also has its challenges. This type of system is a more sensitive representation of gene expression but also can give inaccurate readings if multiple time points are not recorded.

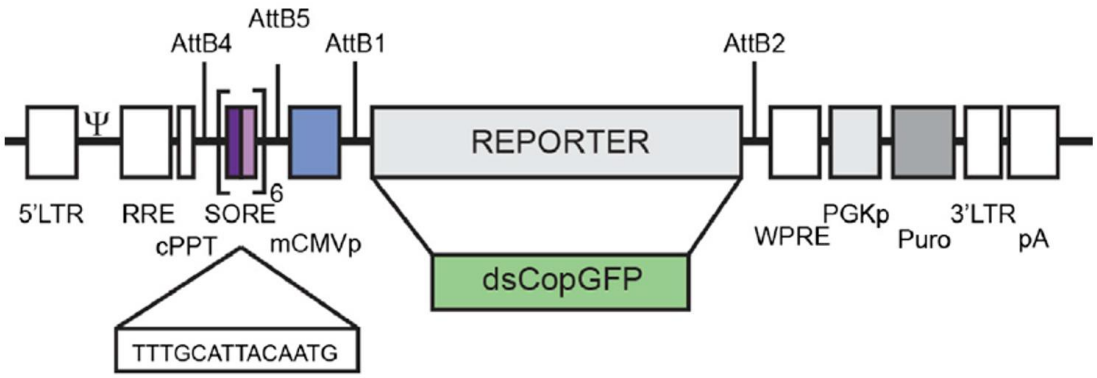

Figure 1. Schematic of lentiviral stem cell reporter SORE6-GFP

Att B1, B2, B4, B5 represent AttB sites for Gateway recombinational cloning. SORE is the SOX2/OCT4 composite response element, present in six copies. mCMVp is the minimal Cytomegalovirus promotor. dsCopGFP is a destabilized green fluorescent protein gene. Puro is a puromycin resistance gene used for puromycin selection. RRE is the rev response element which the rev protein binds. cPPT is the central polypurine tract essential for site recognition of proviral DNA synthesis. WPRE is the woodchuck hepatitis virus post-transcriptional regulatory element which stimulates nuclear export. PGKp is the mammalian promotor phosphoglycerate kinase gene. pA is the polyadenylation signal. 5' and 3' LTRs are involved with reporter integration in host genomeTang et. al.[45]

CHAPTER TWO:

RESULTS

Rationale

Cancer aggressiveness during recurrence in HGSOC and GBM can be attributed to CSCs. Since radiation has been known to enrich for CSCs, we aimed to compare the effects of different radiation types on CSC populations. Our goal was to detect changes in CSC populations, as assessed using a stemness reporter, in response to radiation. To accomplish this, we optimized a lentiviral transduction system to allowed for robust real time detection of individual CSCs via flow cytometry. We confirmed reliability of reporter behavior via RT-qPCR, immunofluorescence microscopy and permeabilized flowcytometry.

Puromycin Selects for Cells Lenti-virally Transduced

The SORE6-GFP plasmid[45] includes a puromycin resistance gene for selection of cells that have been successfully transduced. In order to get an accurate representation of GFP+ cells, incubation in puromycin was necessary to only analyze cells with the reporter. Upon incubating cells for 5 days in puromycin, the lowest concentration at which all non-transduced cells were killed off was 0.33ug/mL for NCCIT, 1ug/mL for LN18, 1ug/mL for T98G, 3ug/mL for OVCAR8, 0.33ug/mL for OVSAHO, 0.1ug/mL for PDX6, 1ug/mL for PDX4, and 0.1ug/mL for MCF7 (Table 1).

Table 1. Puromycin Concentration to select transduced cell line

Cell Line	Puromycin Concentration (ug/mL)
NCCIT	0.33
LN18	1
T98G	1
OVCAR8	3
OVSAHO	0.33
PDX 6	0.1
PDX 4	1
MCF7	0.1

After 5 days of incubating cells with puromycin, the lowest concentration that killed all non-transduced cells is listed above.

Bacterial Transformation of SORE6-GFP Plasmid

To synthesize SORE6-GFP reporter it was inserted into bacteria that would replicate to make more copies of the plasmid. When transforming stbl3 E.coli with M01 (SORE6-GFP), many isolated colonies on LB agar plates with ampicillin were observed which yielded robust transformation success (Fig.1a). In order have a positive control for ampicillin resistance PUC19 cells were plated.

Significant growth for positive control confirmed transformation efficiency (Fig.1b). Two additional plasmids (VSVG and Gag/pol) were also synthesized which were necessary for making virus as VSVG is the gene encoding the viral coat and Gag/pol is responsible for expression of the surface receptor that allows for viral uptake during viral transduction experiments. When E.coli were transformed with VSVG and Gag/pol streak plates showed isolated colonies on LB agar plates with ampicillin indicating successful bacterial transformation (Fig.1c and Fig.1d).

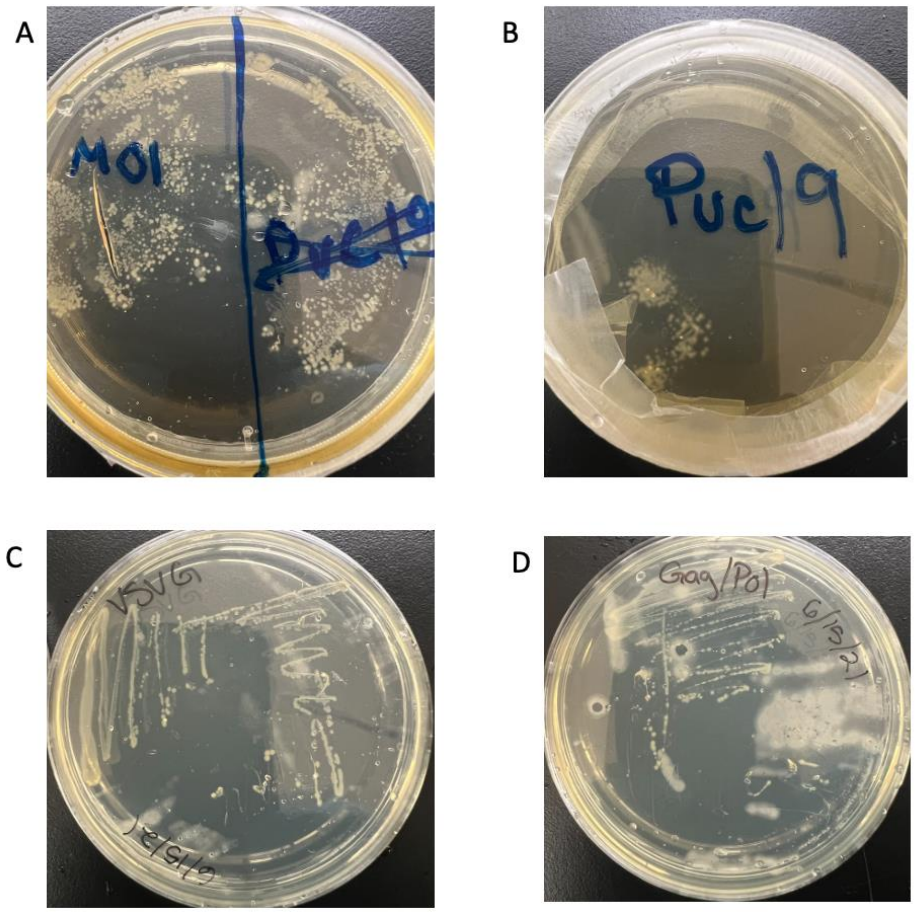

Figure 2. Transformed E. coli Plated on LB Agar with Ampicillin

a.) 25 uL of suspension culture of M01 (SORE6-GFP) transformed cells plated. b.) 25 uL of suspension culture of PUC19 transformed cells spread plated. c.) Streak plate of VSVG transformed cells. d.) Streak plate of Gag/Pol transformed cells.

DNA Digest and Electrophoresis Quality Control Check

After bacteria were transformed and SORE6-GFP plasmid was harvested via miniprep, quality control check was completed via DNA digest and gel electrophoresis. The SORE6-GFP plasmid is 8573 bp in length[45]. ApE software generated a plasmid schematic which was utilized during restriction enzyme digestion (Fig.2a) Upon restriction digest analysis using XhoI, two DNA fragments of 1963bp and 6610bp in length were observed, as expected from XhoI restriction enzyme sites at 3052bp and 5015bp (Fig.2b and Fig.2c).

A

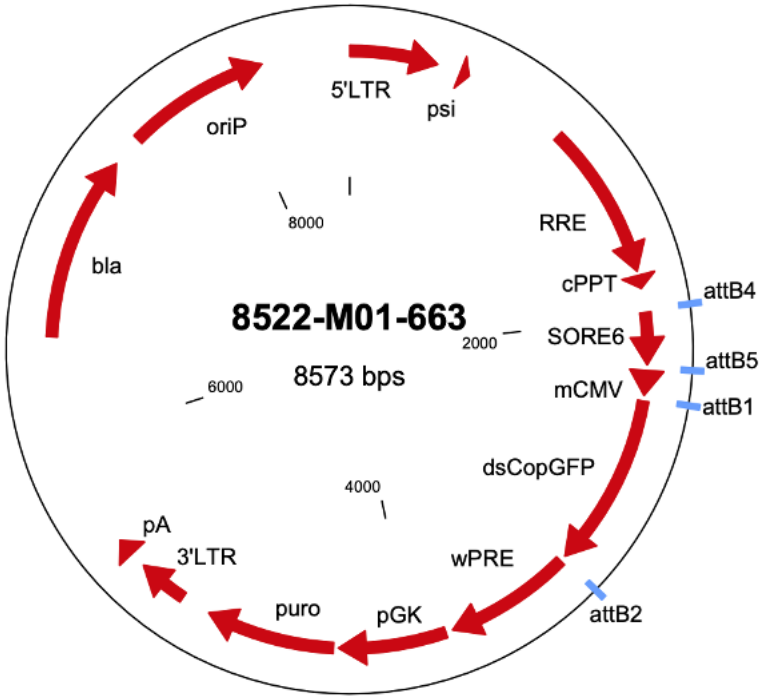
5'LTR
psi
oriP
8000
RRE
bla
cPPT
attB4
8522-M01-663
2000
SORE6
attB5
8573 bps
6000
mCMV
attB1
dsCopGFP
4000
pA
3'LTR
wPRE
puro
pGK
attB2

B

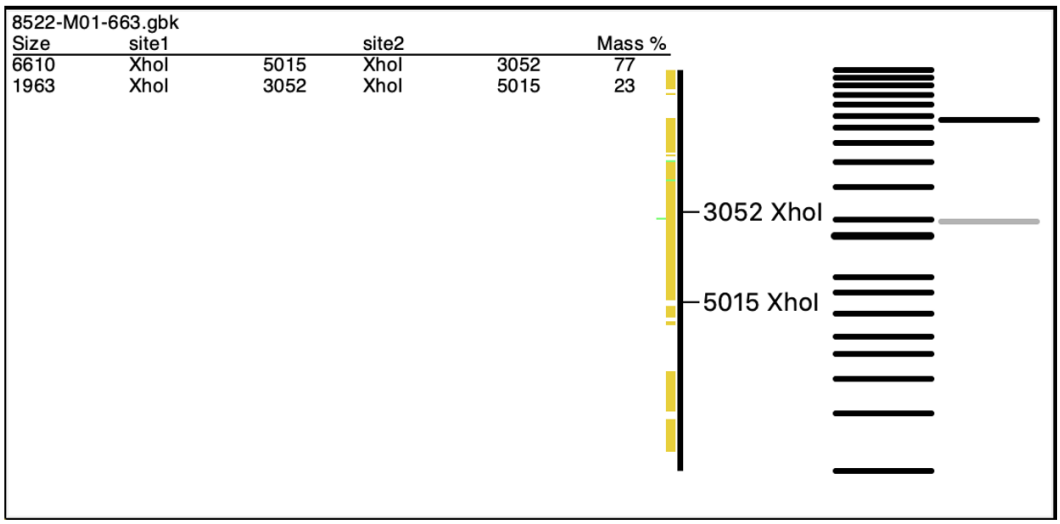
8522-M01-663.gbk
Size site1 site2 Mass %
6610 XhoI 5015 XhoI 3052 77
1963 XhoI 3052 XhoI 5015 23
3052 XhoI
5015 XhoI

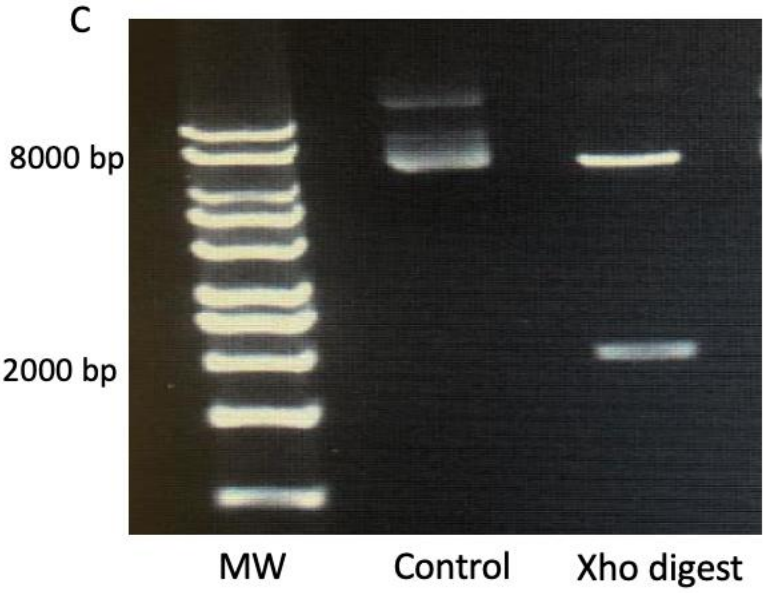

Figure 3. SORE6-GFP Plasmid Quality Control Check via Restriction Enzyme Digest and Gel Electrophoresis

a.) SORE6-GFP reporter plasmid schematic via ApE biosoftware b.) DNA gel electrophoresis predicted with XHO1 restriction enzyme digest via ApE biosoftware c.) DNA gel electrophoresis with 1KB Axygen ladder on far left, control uncut sample in the middle, and XHO1 digest in the right lane.

Cell Panel

Cells for radiation exposure were carefully selected dependent on baseline SORE6-GFP expression. The panel of cells utilized in this study is an accurate representation of both HGSOC and GBM, providing insight into *in vitro* cancer stem cell regulation induced by radiation. A combination of cell lines and patient derived cells was transduced with SORE6-GFP to characterize the Sox2 and Oct4 expression (Table 2). NCCIT was utilized as a positive control for stemness because it has been described to have high levels of pluripotency

transcription factors. Patient derived samples (PDX6 and PDX4) provided insight into cellular behavior that lab adapted cells lines may have lost due to long periods of culturing.

Table 2. Cell Panel Utilized to Characterize Cancer Stem Cell Response to Radiation

Cell Line	Cancer Type	Cell Line/ Xenograft
Ovsaho	High grade serous ovarian cancer	Cell line
Ovcar8	High grade serous ovarian cancer	Cell line
NCCIT	Embryonal Carcinoma	Cell line
LN18	Glioblastoma	Cell line
T98G	Glioblastoma	Cell line
PDX4	High grade serous ovarian cancer	Patient derived xenograft
PDX6	High grade serous ovarian cancer	Patient derived xenograft

Immunofluorescence Microscopy Localizes Stemness Transcription Factor Oct4 in the Nucleus of NCCIT Cells

Since Oct4 is a transcription factor, nuclear localization is expected which was confirmed by immunofluorescence microscopy. Oct4 antibody staining provided robust fluorescence in a high proportion of NCCIT cells. All images were taken at 20x magnification and scale bars represent 25um. The bright field image shows the asymmetrical fibroblastic morphology of NCCIT (Fig. 4a). DAPI

was utilized to stain the nucleus in blue to identify if proteins had nuclear localization (Fig. 4b) Oct4 was stained in green to visualize where the transcription factor was located (Fig. 4c). When images were stacked, we observed that Oct4 was located within the nucleus because the green fluorescence overlayed with the blue DAPI stain (Fig. 4d)

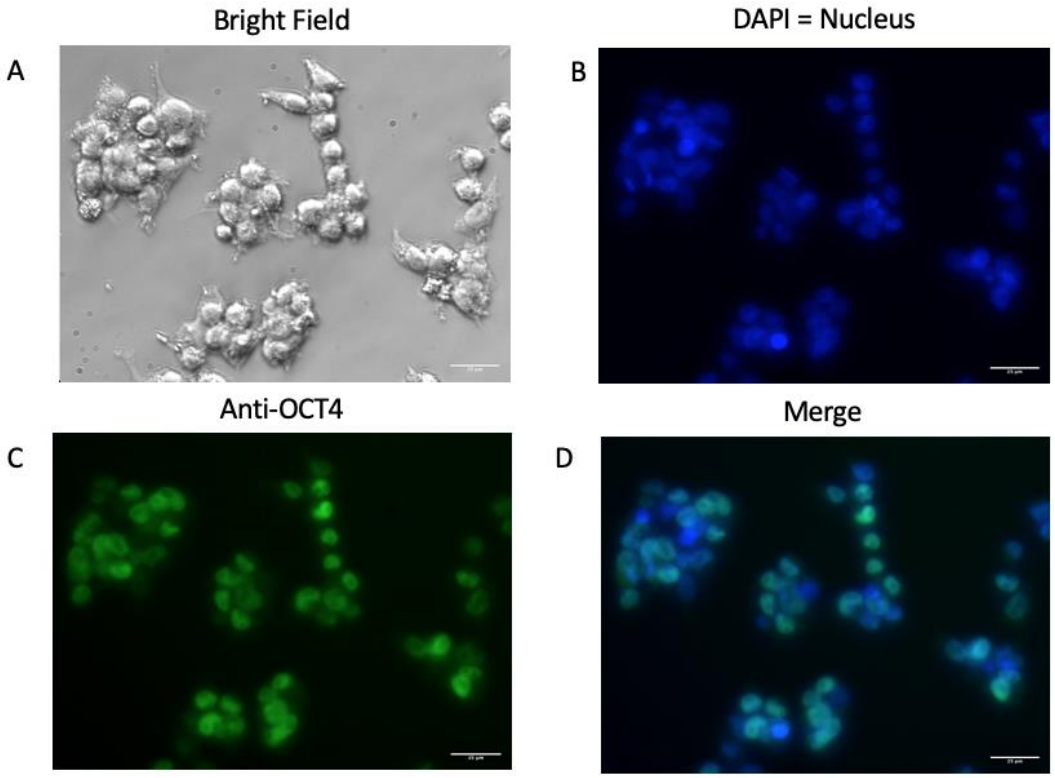

Figure 4. Immunofluorescence Microscopy Nuclear Localization of Oct4

a.) Bright field image of NCCIT under 20x magnification; scale bare represents 25um all images analyzed in ImageJ b.) Nucleus of NCCIT stained with DAPI c.) Oct4 transcription factor stained in green in NCCIT d.) merged images of DAPI and Oct4 in NCCIT.

Permeabilized Flow Cytometry

Antibodies against Oct4 and Sox2 were used to quantify expression of these proteins as a measure of “stemness” in order to analyze reporter activity. After cells were fixed and permeabilized, flow cytometry quantified the proportion of cells stained by each antibody which highlighted cancer stem cells. Isotype control served as a positive control while unstained cells were a negative control. For all antibodies a higher proportion of cells fluoresced in NCCIT compared to D2F as expected because D2F is a differentiated fibroblast cell line (Table 3). With every antibody, there was much more binding between antibody and proteins in NCCIT, the positive control, than in D2F, the negative control, supporting the use of these antibodies for detection of these antigens (Table 3). There was a high degree of variability between the antibodies, which could be accounted for by a few different reasons. One theory is that the affinities between the antibody and the protein antigens are different causing a difference in protein labeling. Each antibody is going to have a different epitope which is going to affect the interaction between the antibody and the protein. We also noticed variability in nonspecific binding with our control samples which would cause differences in background noise of the experiment. The antibodies with the highest percentage of staining were ones where the primary antibody was conjugated to the fluorophore with the exception of Oct4 (c30a3). With these samples the isotype control also had the most binding, indicating that there was background noise which could be lending to the high amount of fluorescence.

NCCIT has a SORE6-GFP expression of 24% which leads us to believe that Oct4(n19) and Sox2 DL488 are the antibodies that give the most accurate representation of cells that are expressing these proteins. For future studies, further antibody validation is warranted.

Table 3. Quantification of Cell Expressing Oct4 and Sox2 Proteins via Antibody Intracellular Staining

	% of Fluorescent Cells	
Antibody	**NCCIT**	**D2F**
Oct4 (n19)	25	7.7
Oct4 (c10)	3.1	0.2
Oct4 AF488	98.1	3.8
Oct4 (c30A3)	87.5	0.4
Sox2 AF 488	85.1	2.8
Sox2 DL488	25.1	1.9

Percentage of fluorescent cells are listed in each column under each cell line (n=1, minimum 2.5 x 10^5 cells).

Gene Expression of Stemness Markers via RT-qPCR

Cells were plated at 8 x 10^4 cells/6well 24 hours prior to exposure to proton and photon radiation and then 72 hours post radiation GFP expression

was measured via flow cytometry analysis. Harvesting cells after radiation to measure transcript production in PDX6 provided another angle of insight into cancer stem cell response within primary tumor cells. Validation of reporter behavior was done via RT-qPCR. An increase of Sox2 expression of 4.1 fold ($p<0.01$) was found but only for proton radiation. When the two radiation types were compared, significant differences were found at 4Gy ($p<0.05$) and 8 Gy ($p<0.01$)(Fig. 3a). An increasing trend in Oct4 expression was observed again only for proton radiation and when radiation types were compared only 2Gy was different ($p<0.05$) (Fig.3b). When stemness marker Lin28 transcripts were measured, a significant change or significant difference between proton and photon radiation was not found (Fig. 3c).

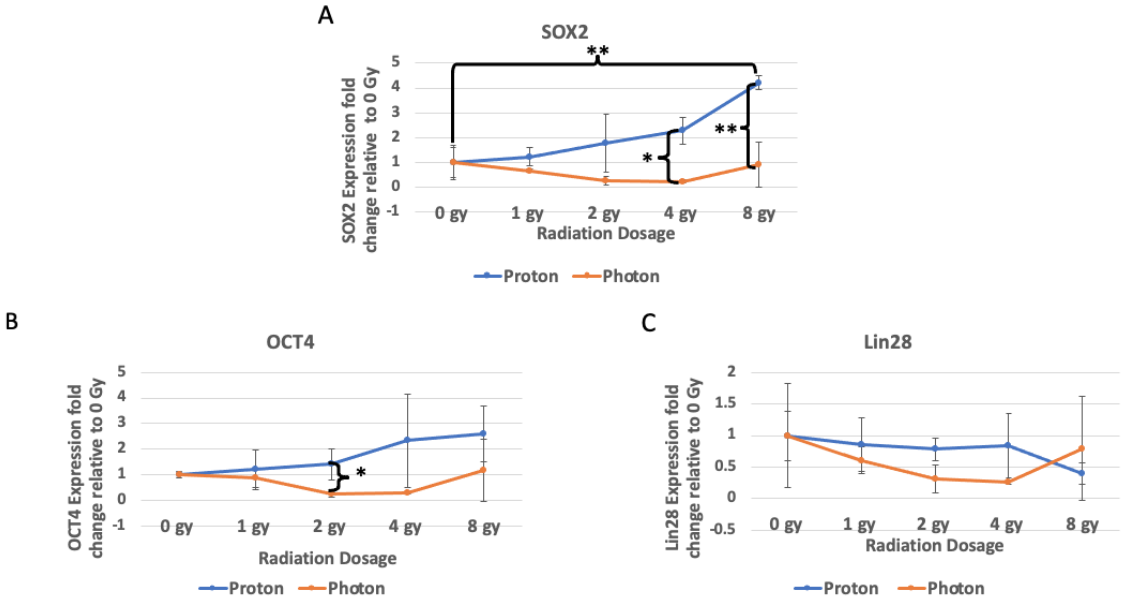

Figure 5. Transcript Analysis of Stemness Markers Sox2, Oct4, and Lin28 in PDX6

a.) Sox2 in response to increasing dosages of proton and photon radiation (n=3).

b.) Oct4 in response to increasing dosages of proton and photon radiation (n=3)

c.) Lin28 in response to increasing to dosages of proton and photon radiation (n=3)

SORE6-GFP in Response to Radiation via Flow Cytometry

Once cells were transduced with SORE6-GFP, cells were plated at 8 x 10^4 cells/6well and exposed to proton and photon radiation. 72 hours post radiation GFP expression was measured via flow cytometry analysis. Utilizing FlowJo, GFP positive cells were gated utilizing the gating scheme below (Fig.6).

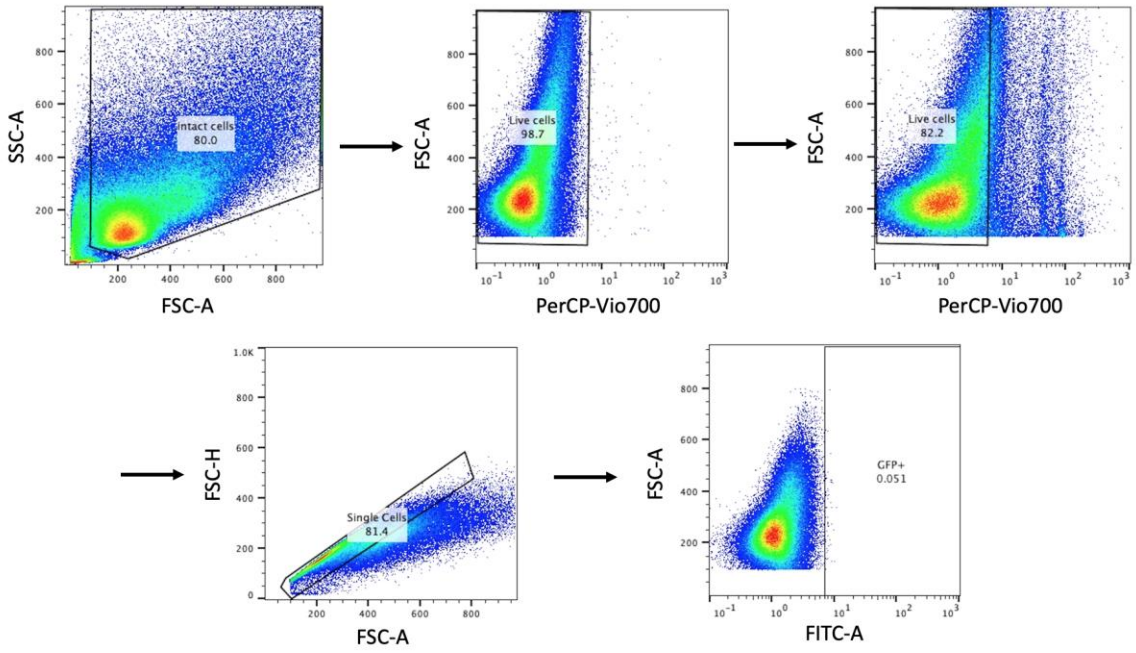

Figure 6. Selecting for Cancer Stem Cells

FlowJo gating scheme to select for GFP+ cells. Intact cells were gated based on FSC-A (cell size) and SSC-A (cell complexity); Live cells were gated based on FSC vs. PerCP because PerCP is the channel that detects signal from 7AAD

viability marker. Single cells were gated based on FSC-H vs. FSC-A; GFP+ cells were gated based in FSC-A vs. FITC.

At the highest dosage of radiation (8Gy), SORE6-GFP significantly increased 1.3 fold ($p<0.001$) in response to photon radiation and significantly increased 1.2 fold ($p<0.001$) in response to proton radiation for LN18 (Fig.7a). The only significant difference between proton and photon SORE6-GFP expression was at 4Gy ($p<0.05$) for LN18 (Fig.7e). When T98G was exposed to radiation, the proportion of SORE6-GFP positive cells increased a maximum of 1.9 fold ($p<0.01$) for proton and 1.5 fold ($p<0.001$)for photon (Fig.7b). When comparing the SORE6-GFP expression between proton and photon radiation there were no differences between the two (Fig.7f). PDX4 responded to proton radiation with increases in SORE6-GFP positive cells maximally at 8Gy with 2.7 fold ($p<0.01$) for proton and photon radiation 3.1 fold ($p<0.0001$) (Fig.7c). The two radiation types showed no significant differences at all radiation dosages for PDX4 (Fig.7g). OVSAHO increased in proportion of SORE6-GFP positive cells a maximum of 1.8 fold ($p<0.0001$) for both radiation types (Fig.7d). When the two radiation types were compared for OVSAHO, a significant difference in SORE6-GFP expression at 2Gy ($p<0.05$) was observed (Fig.7h)

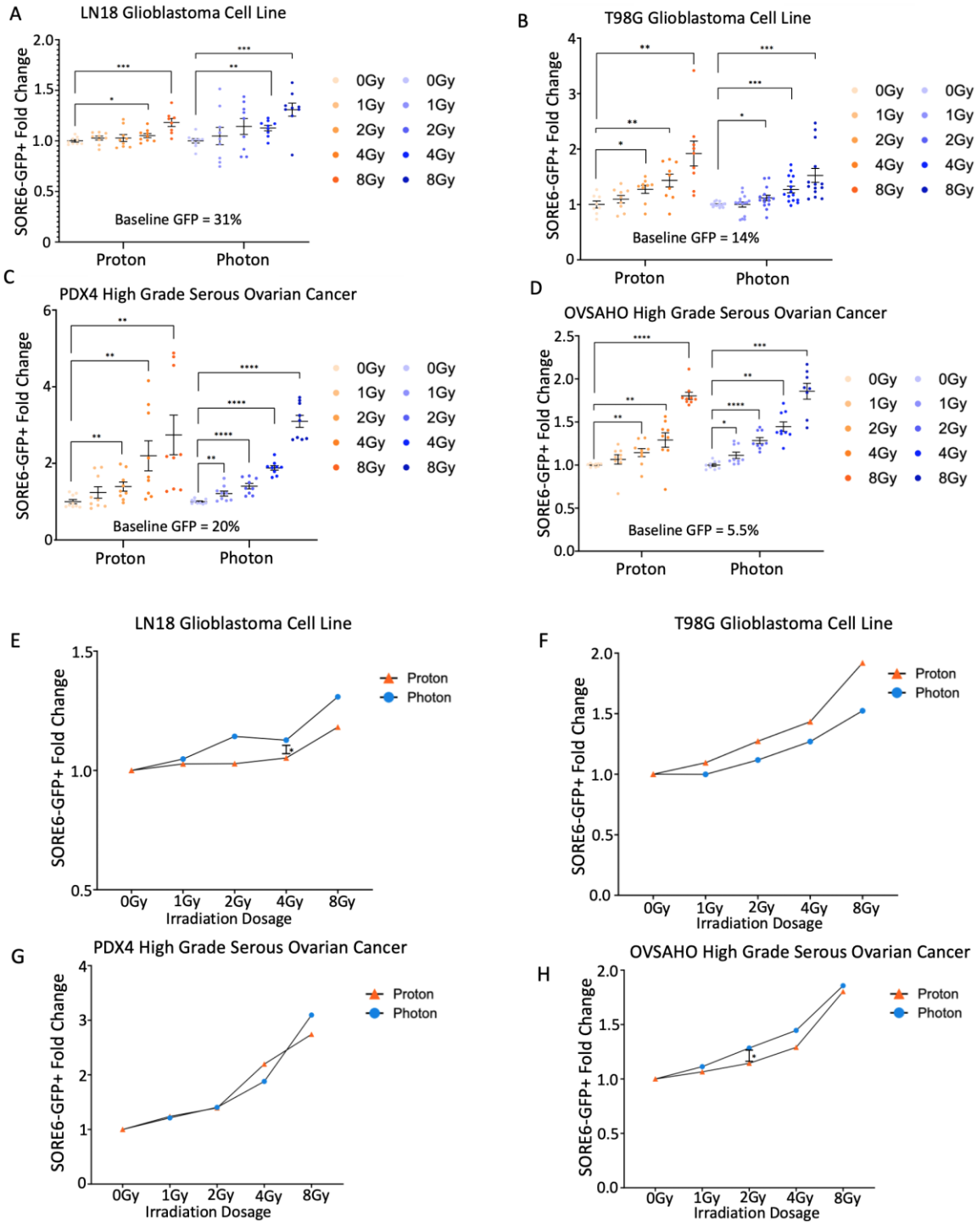
A
LN18 Glioblastoma Cell Line
SORE6-GFP+ Fold Change
Baseline GFP = 31%
Proton
Photon
0Gy
1Gy
2Gy
4Gy
8Gy
B
T98G Glioblastoma Cell Line
Baseline GFP = 14%
C
PDX4 High Grade Serous Ovarian Cancer
Baseline GFP = 20%
D
OVSAHO High Grade Serous Ovarian Cancer
Baseline GFP = 5.5%
E
LN18 Glioblastoma Cell Line
Irradiation Dosage
F
T98G Glioblastoma Cell Line
G
PDX4 High Grade Serous Ovarian Cancer
H
OVSAHO High Grade Serous Ovarian Cancer

Figure 7. SORE6-GFP Activity in Response to Proton and Photon Irradiation

a.) Flow cytometry analysis of average SORE6-GFP expression in LN18 after 72 hours of proton and photon radiation exposure comparing dosages (n=9). b.) Flow cytometry analysis of average SORE6-GFP expression in T98G after 72 hours of proton and photon radiation exposure comparing dosages (n=9). c.) Flow cytometry analysis of average SORE6-GFP expression in PDX4 after 72 hours of proton and photon radiation exposure comparing dosages (n=9) d.) Flow cytometry analysis of average SORE6-GFP expression in OVSAHO after 72 hours of proton and photon radiation exposure comparing dosages (n=9) e.) Flow cytometry analysis of average SORE6-GFP expression in LN18 72 hours after proton and photon radiation exposure comparing radiation types (n=9) f.) Flow cytometry analysis of average SORE6-GFP expression in T98G 72 hours after proton and photon radiation exposure comparing radiation types (n=15) g.) Flow cytometry analysis of average SORE6-GFP expression in PDX4 72 hours after proton and photon radiation exposure comparing radiation types (n=9) h.) Flow cytometry analysis of average SORE6-GFP expression in OVSAHO 72 hours after proton and photon radiation exposure comparing radiation types (n=9).

CHAPTER THREE:

MATERIALS AND METHODS

Cell Culture

All studies were approved by the Loma Linda University (LLU) Institutional Review Board (IRB). Deidentified fresh ovarian cancer samples were provided by the Loma Linda University Cancer Center Biospecimen Laboratory (LLUCCBL). Patient-derived samples were cultured in 75% Ham's F12 media (Cytiva) and 25% Dulbecco's Modified Eagles Medium (DMEM) (Cytiva) 4.5 g/L glucose (Biomatik) supplemented with 5% fetal bovine serum (FBS) (Omega Scientific), 10uM insulin (Sigma Aldrich), 0.4 ug/mL hydrocortisone (Sigma Aldrich), 2 ug/mL isoprenaline (Sigma Aldrich), 24 ug/mL adenine (Sigma Aldrich), and 1% penicillin-streptomycin (Genesee Scientific).

OVCAR8 and OVSAHO cells were cultured in Dulbecco's Modified Eagles Medium (DMEM) 4.5 g/L glucose with 10% FBS, 2 mM L-Glutamine (Genesee Scientific), and 1% penicillin-streptomycin.

LN18 cells were cultured in DMEM 4.5 g/L glucose supplemented with 5% FBS, 1% penicillin, and 1% streptomycin.

T98G cells were cultured in E-MEM (Genesee Scientific) supplemented with 10% FBS, 1% penicillin, and 1% streptomycin.

NCCIT cells were cultured in RPMI (Cytiva) supplemented with 10% FBS, 2mM L-glutamine, 1mM sodium pyruvate (Fisher Scientific), 1% Non-essential amino acids (Cytiva), 1% penicillin, and 1% streptomycin.

Lenti-x 293T cells were cultured in DMEM with 4.5 g/L glucose, 3.7 g/L sodium bicarbonate (Cytiva) supplemented with 10% FBS, 1% L-Glutamine, 1% penicillin, 1% streptomycin, 1% sodium pyruvate.

MCF7 cells were cultured in MEM (Cytiva) supplemented with 10% FBS, 0.01 mg/mL human recombinant insulin (ATCC) (Sigma Aldrich), 1% penicillin, and 1% streptomycin.

Bacterial Transformation

All microbiology work was performed near a Bunsen burner within the circle of sterility. Stbl3 E.coli were thawed on ice. 25 uL of stlb3 cells were transferred to a sterile Eppendorf tube. Next, 2-3 uL of DNA was added to stbl3 cells. The Eppendorf tube was flicked and incubated on ice for 30 minutes. Cells were heat shocked at 42C for exactly 45 seconds. Cells were incubated on ice for 2 minutes. 300 uL of SOC was added. Cells were put on shaker for 30-60 minutes at 150 RPM. Cells were spread plated on LB plates containing 1% ampicillin. Plates were incubated overnight.

Miniprep

All minipreps were performed according to the “High Yield Miniprep” protocol using Qiagen solutions. Once cells were incubated overnight, several colonies were grown in 3 mL suspension cultures containing 1% ampicillin. All but 250 uL of suspension culture was transferred to Eppendorf tubes and centrifuged at 6000 RPM for 5 minutes. Supernatant was decanted. Pellet was resuspended in 150 uL of cold P1 buffer. Next, 150 uL of P2 buffer was added and Eppendorf

tubes were inverted 6 times. 150 uL of P3 buffer was then added and Eppendorf tubes were inverted 6 times. Eppendorf tubes were incubated on ice for 10 minutes. After incubation, Eppendorf tubes were inverted one time and centrifuged for 10 minutes at 14000 g at 4 C. Supernatant containing the DNA was transferred to a sterile Eppendorf tube. 315 uL of 100% isopropyl alcohol was then added to supernatant and inverted once. Next, solution was incubated on ice for 15 minutes. Then solution was centrifuged for 30 minutes at 14000 g at 4 C. Supernatant was then discarded. 1 mL of 70% ethanol was added to DNA pellet and inverted once. Eppendorf tubes were then centrifuged for 10 minutes at 14000 g at 4 C. Ethanol was then decanted and the tube was inverted on a kimwipe to dry for 5 min. DNA was resuspended in 50 uL of molecular grade water and stored at -20 C.

DNA Digest and Gel Electrophoresis

2 uL of DNA from miniprep was added to 0.5 uL of restriction enzyme, 2 uL of 10x fast digest buffer, and brought up to a total volume of 20 uL with molecular grade water, and digested for 30 min at 37 degrees C. 10 uL of solution was then run on 1.5% agarose gel for 15-30 minutes at 100 mAMPS. All gel images were then captured on alpha imager.

Maxiprep

All maxipreps were performed according to the Qiagen Maxiprep Kit (Ref. # 12362).

293T Transfection for Production of Lentivirus

24 hours before transfection Lenti-x 293T cells were plated on a 15 cm dish at 60-80% confluency. Into an Eppendorf, 7.5 ug of reporter plasmid, 6ug of lenti gag/pol plasmid, and 2.25 ug of VSVG plasmid were combined. Plasmids were incubated at 50 C for 5 minutes to kill any bacteria. 465 uL of 7.5 mM Polyethylenimine (PEI) 7.5 mM monomer unit, pH 8.0 (25000MV polyscience) and 535 uL of 150 mM sodium chloride was combined. Plasmid solution was brought up to 1 mL with 150 mM sodium chloride. PEI sodium chloride solution was mixed with plasmid sodium chloride solution and was vortexed for 10 seconds then was incubated for 10-15 minutes. Solution was then added dropwise to 15 cm dishes. 24 hours later, a media change was performed on the Lenti-x cells. 24 hours after media change, media was harvested, centrifuged at 1500 rpm for 5 minutes, filtered and 150 mM polyethylene glycol (PEG) was added, then stored overnight at 4 C. 24 hours after first media harvest, a second media harvest was performed in the same fashion. Virus was then concentrated by centrifuging at 2500 RPM for 20 minutes. All but 200 uL was aspirated and centrifuged for 5 minutes at 1500 RPM. All media was aspirated and viral pellet was resuspended in 200 uL of optimem (Fisher Scientific) then transferred to a cryovial and stored at -70 C. Viral titration was then performed by adding 0uL, 0.3uL, 1uL, 3uL, 9uL, 27uL into each well of a 6 well with $2x10^5$ LentiX cells and analyzed by flow cytometry to determine viral titers.

Viral Transduction of Cell Lines and Patient Samples

To 10^5 cells 6 ug/mL of protamine sulfate was added and then appropriate amount of lentivirus was added and shaken to create a homogenous mixture. 24 hours later, media was changed. 36 hours after transduction, puromycin was added for selection and allowed to incubate for 3-5 days.

Irradiation

Proton Irradiation

Cells were subject to irradiation utilizing a therapeutic proton beam completed at the James M. Slater Proton Treatment and Research Center, Loma Linda California. Irradiations consisted of 250 MeV protons and were modulated to generate a 5.0 cm wide spread-out Bragg peak (SOBP). The cells were located at a water equivalent depth of 29.6 cm, specified using CIRS plastic water blocks, which placed the cells in the uniform dose SOBP region of the proton dose profile. Irradiations were conducted with the beam incident on the underside of the flask to ensure accurate placement of the cell layer with respect to the proton depth dose profile. The proton field size employed for the irradiation of the cells was circular with an 18 cm diameter. Protons were delivered from our synchrotron accelerator in a pulsed fashion, with a pulse duration of 0.125 seconds and a duty cycle of 2.2 seconds. This pulsed modality of beam delivery gave a dose rate of approximately 0.8 Gy/min and cells were exposed to single doses of 0, 1, 2, 4, and 8 Gy. Proton radiation was performed according to Boyle et. al., 2018[46].

Photon Irradiation

Cells underwent photon irradiation using a Co^{60} irradiator (Eldorado Model 'G' machine, Atomic Energy of Canada Ltd., Commercial Products Division, Ottawa, Canada) with a dose rate of 1Gy/min at 80cm source to sample distance (SSD) and field size of 40x40 cm^2. Photon radiation was performed according to Pariset et. al., 2020[47].

Thawing and Cryopreservation

All cells were thawed from liquid nitrogen by water bath and transferred to 10 mL of media. Cells were centrifuged at 1250 RPM for 5 minutes. Supernatant was then aspirated and cells were resuspended in 1 mL of media and transferred to appropriate growth flask. Appropriate amount of media was added and cells were put in incubator.

All cells were cryopreserved after single cell suspension was made. Appropriate amount of cell suspension was transferred to an Eppendorf tube and centrifuged at 1250 rpm for 5 minutes. Media was then aspirated and pellet was resuspended in 200 uL of media to be transferred to a cryovial. 300 uL of freeze media (FBS and 5% DMSO) was added to cryovial and stored in Mr. Frosty at -70 C. 24 hours later cells were transferred to liquid nitrogen.

Flow Cytometry

After trypsinization and cell counting, cells were placed in FACS stain (500mL PBS, 1% FBS, 0.1% NaN_3, and 2mM EDTA) and incubated with 7AAD viability dye in the dark for 15 minutes. GFP expression was analyzed using the

MACSQuant Analyzer 10 (Miltenyi Biotec, Auburn, Ca, USA). All flow cytometry data was analyzed via FlowJo.

RT-qPCR

Total RNA from cell culture samples was isolated using Trizol reagent (Life Technologies, Carlsbad, CA) according to the manufacturers protocol. 1 ug of RNA was utilized to synthesize cDNA using Maxima first strand synthesis kit (K1672; ThermoFisher Scientific, Grand Island, NY, USA). RT-qPCR for mRNA was performed using PowerUP SYBR Green master mix (ThermoFisher Scientific, Grand Island, NY, USA) and specific primers on the Stratagene Mx3005P thermocycler (Agilent Technology, Santa Clara, CA, USA) All data was analyzed using delta delta method and normalized to actin.

Immunofluorescence Microscopy

Cells were plated at 60-70% confluency in 24 well plates. Once adhered, media was aspirated and wells were washed with 200 uL of PBS. Cells were then fixed with 4% Paraformaldehyde and incubated for 15 minutes at room temperature. After incubation, cells were washed gently 3x with PBS. Next, cells were permeabilized with PS+ (90 mL of DMEM with 4.5 g/L glucose, 10% goat serum, 0.1% triton X-100, 10 mM HEPES pH 7.4, and 10 mM glycine) and incubated for 30 minutes at room temperature. PS+ was aspirated and primary antibody at appropriate dilution in PS+ was added. Primary antibody was incubated for 3 hours at room temperature. Cells were then washed 3x with PS+ and secondary antibody at appropriate dilution in PS+ was added then incubated for 3 hours at

room temperature. Next, cells were washed 3x with PS+. DAPI was then added at appropriate dilution in PS+ and incubated for 15 minutes at room temperature. Cells were washed 1x with PBS and observed under fluorescent microscope (Nikon Eclipse Ti).

Permeabilized Flow Cytometry

Cells were harvested at $1x10^6$ cells/96well and centrifuged at 1500rpm for 5 minutes. Media was aspirated and cells were resuspended in 100uL of 4% paraformaldehyde. Cells were mixed well to dissociate pellet and prevent cross-linking of individual cells. Cells were incubated at 20-25°C for 15 minutes. Cells were centrifuged at 1500 rpm for 5 minutes and washed with excess 1x PBS. Supernatant was discarded and cells were resuspended in 100uL of cell permeabilization buffer (30uL of triton x-100 to a final concentration of 0.3% and 10mL of PBS with 0.5 g bovine serum albumin). Cells were incubated at 20-25°C for 10 minutes. Cells were centrifuged at 1500 rpm for 5 minutes and resuspended in 100 uL of primary antibody prepared in antibody dilution buffer (10mL of PBS with 0.5g bovine serum albumin) at manufacture recommended dilution factors listed next. (Oct4 (n19) Santa Cruz SC-8360 (1:50), Oct4 (c10) Santa Cruz Biotechnology SC-5279 (1:50), Oct4 AF488 BD Biosciences 560253 (1:5), Sox2 AF488 BD Biosciences 560301(1:20), Sox2 DL488 Novus Biological NB110-79875g (1:30), Oct4(c30a3) Cell Signaling Technology 2840 (1:100). Cells were incubated at 20-25°C for 60 minutes. Next, cells were washed 2 times with 1x PBS. Cells were resuspended in 100uL of diluted fluorochrome-

conjugated secondary antibody prepared in antibody dilution buffer at recommended dilution factor (all antibodies secondary antibodies were diluted 1:300). Incubation of secondary antibodies was at 20-25°C for 30 minutes protected from light. Cells were washed twice with 1x PBS, resuspended in 200 uL of 1x PBS, and analyzed via flow cytometry.

CHAPTER FOUR:

DISCUSSION

Cancer stem cells have become an increasingly popular therapeutic target for modulating cancer recurrence because they are known to have tumor initiating and recapitulating abilities[48]. Challenges present themselves when investigators began to realize CSC express heterogeneous biomarkers between cancer types[49]. This means that not all malignancies can be treated the same and characterization is required to develop personalized clinical care plans for each patient. Biomarker expression is only part of understanding how to combat CSCs; CSC behavior needs to also be taken into consideration when attempting to eradicate these small subpopulations with the tumor. Monitoring the growth of a tumor in real time is going to provide a fundamental understanding of modulating CSC to inhibit post treatment aggressiveness especially in cancer with high recurrence rates such as HGSOC and GBM.

In this study, we optimized a Sox2/Oct4 GFP based reporter to evaluate how CSCs are regulated in response to proton and photon radiation in HGSOC and GBM in vitro models. We utilized two HGSOC cell lines, two HGSOC PDXs, two GBM cell lines, and an embryonal carcinoma cell line previously described to have high level of Sox2/Oct4 that we modeled as our positive control (Table 2). Even though proton and photon radiation are very different, we hypothesize that the effects of proton and photon radiation will be similar in terms of CSC

response which was investigated via flowcytometry, RT-qPCR, and intracellular staining.

In order to analyze the effects of radiation on CSCs, we first needed to grow up our SORE6-GFP plasmid in E.coli bacteria. By transforming bacteria with the plasmid, we are able to harness bacterial mitosis to synthesize copies of the plasmid. Since the transformation process is not 100% efficacious, we spread plated to isolate colonies and select for positively transformed bacteria. We observed robust isolated colony growth for not only SORE6-GFP transformed bacteria but also VSVG (viral coat) and Gag/pol (surface receptor responsible for viral uptake) transformed bacteria (Figure 1). Next, we extracted the plasmids from the bacteria via miniprep and ran a quality control check via DNA gel electrophoresis post restriction enzyme digest. Since our plasmid is 8573 bp (Figure 2a), we digested with XHO1 restriction enzyme which has cut sites at 3052bp and 5015bp resulting in two DNA fragments of 1963bp and 6610bp in length (Figure 2b). We observed distinct bands at expected fragment lengths confirming our transformation was successful (Figure 2c). At this point, we transfected Lenti-X cells with VSVG, Gag/pol, and SORE6-GFP for production of lentivirus. After harvesting virus, we transduced the cells we wanted to observe changes in CSCs in response to radiation. In order to characterize the lowest of concentration of puromycin to select for positively transduced cell lines, we ran kill curves (Table 1).

Sox2 and Oct4 are transcription factors responsible for stemness which are expected to be located in the nucleus. To confirm location of these proteins in our invitro models, we utilized immunofluorescence microscopy to target Oct4. We observed distinct intranuclear staining of Oct4 in NCCIT supporting that this transcription factor is expressed in detectable amounts (Figure 4). Furthermore, we wanted to look at Sox2 and Oct4 protein on an individual cell basis so that we could define reporter activity as we moved to radiation experiments. We ran a panel of four Oct4 and two Sox2 antibodies, to stain these proteins in both NCCIT and D2F cells. We observed a high degree of variability in our antibody panel could be from either the success of antibodies entering the cell post permeabilization or differences in affinity between the antibody and the protein. However, we did confirm that NCCIT consistently had higher Sox2/Oct4 expression when compared to D2F as expected because D2F is a differentiated fibroblast cell line (Table 3). To look at gene expression of Sox2 and Oct4 from a different dynamic, we also measured transcript expression on PDX6 in response to proton and photon radiation. Both Sox2 significantly increased and Oct4 trended upward in response to proton radiation but virtually no change was seen when exposed to photon radiation (Figure 3a and 3b). Now that we know gene expression change of Sox2 and Oct4 occurs in response to radiation, we wanted to measure this change via SORE-GFP.

In order to analyze only the SORE6-GFP cells, we utilized Flowjo after flowcytometry was done on irradiated cells. Once we gated out any cellular

debris with the FCS-A vs SSC-A gate, we gated for live cells by over laying 7AAD negative gate onto the wells that contained 7AAD which indicated where our live cells lie on the FSC-A vs PercP-A gate. Now that we have selected for live cells which are 7AAD negative, we gated for single cells on FSC-A vs FSC-H. The last gate is FSC-A vs FITC-A which indicates how many GFP positive cells we have in our population (Figure 5). Upon statistical analysis, we observed significant increases in CSCs measured by SORE6-GFP for all GBM and HGSOC cells in response to increasing dosages of radiation (Figure 7A, 7B, 7C, 7D). This possibly indicates that radiation is upregulating CSCs which can then drive recurrent aggressiveness in GBM and HGSOC. When we compared the effects between proton and photon radiation, we generally saw no difference in CSCs regulation for all cells (Figure 7E, 7F, 7G, 7H) despite significant differences at 4Gy for LN18 ($p<0.05$) and 2Gy for OVSAHO ($p<0.05$). This goes to support our hypothesis that proton and photon radiation have similar effects on CSC populations.

Proton radiation is thought to be less destructive to normal tissue compared to photon radiation because it is more directed towards the tumor target and less residual radiation is deposited to the surrounding tissue. However, the effects of proton radiation on stemness have not been characterized until now. Comparing the effects of proton radiation and photon radiation in terms of this phenotype should lead to a better understanding of cancer aggressiveness. Knowing the risks and benefits of these two radiation

types will help oncologists design and develop custom personal care approaches when treating different cancer types.

HGSOC and GMB tumor cells tend to infiltrate and invade surrounding tissue[50] which can lead to incomplete resection and recurrence after treatment. Evidence for CSC in response to irradiation in terms of HGSOC and GBM is not clearly understood. The goal of this study was to investigate the effects of irradiation CSC.

This study benefits basic biochemistry science by optimizing the SORE6-GFP system because this can serve to supplement, if not substitute for time consuming and expensive RT-qPCR as well as immunocytochemistry. This reliable reporter system can indicate dynamic changes in CSC populations in real time, giving insight into cancer aggressiveness both *in vitro* and *in vivo*. Now that we know that CSCs are increased in response to irradiation that reporter approach can be taken into animal models show trace where the CSCs are moving throughout the body.

Tumor recurrence and metastases are primarily caused by CSCs which contribute greatly for the poor prognosis in GBM and HGSOC patients. Currently there are no therapeutics specifically targeting CSCs within HGSOC or GBM. This study aimed to develop a clinically relevant therapeutic for targeting CSCs.

Next steps with the reporter would be to characterize other classic stem cells markers such as ALDH, CD44, and CD117 to see if the reporter matches up with other genes noted of the CSC phenotype. From there, optimizing fluorescent

activated cell sorting experiments would be useful to separate GFP positive cells from GFP negative cells then run subsequent CSC functional assays such as spheroid and colony formation to better understand CSC behavior. In the future, there is room for development of mesoporous silica nanoparticles as a delivery method for small RNAs to inhibit the CSC phenotype therefore combatting radiation induced aggressiveness and introducing a novel approach to supplement radiation therapy.

REFERENCES

1. Ahmed, N., Abubaker, K., Findlay, J. & Quinn, M. Cancerous ovarian stem cells: Obscure targets for therapy but relevant to chemoresistance. *Journal of Cellular Biochemistry* **114**, 21–34 (2013).
2. Lathia, J. D., Mack, S. C., Mulkearns-Hubert, E. E., Valentim, C. L. L. & Rich, J. N. Cancer stem cells in glioblastoma. *Genes Dev* **29**, 1203–1217 (2015).
3. Wen, P. Y. *et al.* Glioblastoma in adults: a Society for Neuro-Oncology (SNO) and European Society of Neuro-Oncology (EANO) consensus review on current management and future directions. *Neuro Oncol* **22**, 1073–1113 (2020).
4. Xavier, M.-A., Rezende, F., Titze-de-Almeida, R. & Cornelissen, B. BRCAness as a Biomarker of Susceptibility to PARP Inhibitors in Glioblastoma Multiforme. *Biomolecules* **11**, 1188 (2021).
5. Mirza, M. R. *et al.* The forefront of ovarian cancer therapy: update on PARP inhibitors. *Annals of Oncology* **31**, 1148–1159 (2020).
6. Moore, K. *et al.* Maintenance Olaparib in Patients with Newly Diagnosed Advanced Ovarian Cancer. *New England Journal of Medicine* **379**, 2495–2505 (2018).
7. Markman, M. *et al.* Duration of response to second-line, platinum-based chemotherapy for ovarian cancer: implications for patient management and clinical trial design. *J Clin Oncol* **22**, 3120–3125 (2004).

8. Liao, Q. *et al.* A preliminary study on the radiation-resistance mechanism in ovarian cancer. *Journal of Cancer Research and Therapeutics* **9**, 22 (2013).
9. Fujita, M., Yamada, S. & Imai, T. Irradiation induces diverse changes in invasive potential in cancer cell lines. *Semin Cancer Biol* **35**, 45–52 (2015).
10. Lee, L. & Matulonis, U. Immunotherapy and radiation combinatorial trials in gynecologic cancer: A potential synergy? *Gynecol Oncol* **154**, 236–245 (2019).
11. Kim, W. *et al.* Cellular Stress Responses in Radiotherapy. *Cells* **8**, 1105 (2019).
12. Herrera, F. G., Irving, M., Kandalaft, L. E. & Coukos, G. Rational combinations of immunotherapy with radiotherapy in ovarian cancer. *Lancet Oncol* **20**, e417–e433 (2019).
13. Majidpoor, J. & Mortezaee, K. The efficacy of PD-1/PD-L1 blockade in cold cancers and future perspectives. *Clin Immunol* **226**, 108707 (2021).
14. Walle, T. *et al.* Radiation effects on antitumor immune responses: current perspectives and challenges. *Ther Adv Med Oncol* **10**, 1758834017742575 (2018).
15. Alterations in mitochondrial structure and function are early events of dexamethasone-induced thymocyte apoptosis. *J Cell Biol* **130**, 157–167 (1995).

16. Gupta, K. *et al.* Radiation Induced Metabolic Alterations Associate With Tumor Aggressiveness and Poor Outcome in Glioblastoma. *Front Oncol* **10**, 535 (2020).
17. Randall, E. C. *et al.* Localized metabolomic gradients in patient-derived xenograft models of glioblastoma. *Cancer Res* **80**, 1258–1267 (2020).
18. Lin, H. *et al.* Fatty acid oxidation is required for the respiration and proliferation of malignant glioma cells. *Neuro Oncol* **19**, 43–54 (2017).
19. Moncharmont, C. *et al.* Radiation-enhanced cell migration/invasion process: a review. *Crit Rev Oncol Hematol* **92**, 133–142 (2014).
20. Arnold, C. R., Mangesius, J., Skvortsova, I.-I. & Ganswindt, U. The Role of Cancer Stem Cells in Radiation Resistance. *Front Oncol* **10**, 164 (2020).
21. Ghisolfi, L., Keates, A. C., Hu, X., Lee, D. & Li, C. J. Ionizing radiation induces stemness in cancer cells. *PLoS One* **7**, e43628 (2012).
22. Ramakrishnan, V. *et al.* Radiation-induced extracellular vesicle (EV) release of miR-603 promotes IGF1-mediated stem cell state in glioblastomas. *EBioMedicine* **55**, 102736 (2020).
23. Park, J.-H. *et al.* Radiation-Activated PI3K/AKT Pathway Promotes the Induction of Cancer Stem-Like Cells via the Upregulation of SOX2 in Colorectal Cancer. *Cells* **10**, 135 (2021).
24. Batlle, E. & Clevers, H. Cancer stem cells revisited. *Nat Med* **23**, 1124–1134 (2017).

25. Yu, Z., Pestell, T. G., Lisanti, M. P. & Pestell, R. G. Cancer Stem Cells. *Int J Biochem Cell Biol* **44**, 2144–2151 (2012).
26. Sistigu, A., Musella, M., Galassi, C., Vitale, I. & De Maria, R. Tuning Cancer Fate: Tumor Microenvironment's Role in Cancer Stem Cell Quiescence and Reawakening. *Front Immunol* **11**, 2166 (2020).
27. Shen, S. *et al.* A nanotherapeutic strategy to overcome chemotherapeutic resistance of cancer stem-like cells. *Nat. Nanotechnol.* **16**, 104–113 (2021).
28. Bao, S. *et al.* Glioma stem cells promote radioresistance by preferential activation of the DNA damage response. *Nature* **444**, 756–760 (2006).
29. Nishida, N., Yano, H., Nishida, T., Kamura, T. & Kojiro, M. Angiogenesis in Cancer. *Vasc Health Risk Manag* **2**, 213–219 (2006).
30. Yang, L. *et al.* Targeting cancer stem cell pathways for cancer therapy. *Signal Transduct Target Ther* **5**, 8 (2020).
31. Calabrese, C. *et al.* A Perivascular Niche for Brain Tumor Stem Cells. *Cancer Cell* **11**, 69–82 (2007).
32. Ping, Y.-F., Zhang, X. & Bian, X.-W. Cancer stem cells and their vascular niche: Do they benefit from each other? *Cancer Letters* **380**, 561–567 (2016).
33. Jinushi, M. *et al.* Tumor-associated macrophages regulate tumorigenicity and anticancer drug responses of cancer stem/initiating cells. *Proc Natl Acad Sci U S A* **108**, 12425–12430 (2011).

34. Janiszewska, M. *et al.* Imp2 controls oxidative phosphorylation and is crucial for preserving glioblastoma cancer stem cells. *Genes Dev* **26**, 1926–1944 (2012).
35. Pastò, A. *et al.* Cancer stem cells from epithelial ovarian cancer patients privilege oxidative phosphorylation, and resist glucose deprivation. *Oncotarget* **5**, 4305–4319 (2014).
36. Singh, S. K. *et al.* Identification of human brain tumour initiating cells. *Nature* **432**, 396–401 (2004).
37. Liu, G. *et al.* Analysis of gene expression and chemoresistance of CD133+ cancer stem cells in glioblastoma. *Mol Cancer* **5**, 67 (2006).
38. Friel, A. M. *et al.* Functional analyses of the cancer stem cell-like properties of human endometrial tumor initiating cells. *Cell Cycle* **7**, 242–249 (2008).
39. Baba, T. *et al.* Epigenetic regulation of CD133 and tumorigenicity of CD133+ ovarian cancer cells. *Oncogene* **28**, 209–218 (2009).
40. Ferrandina, G. *et al.* Expression of CD133-1 and CD133-2 in ovarian cancer. *Int J Gynecol Cancer* **18**, 506–514 (2008).
41. Ferrandina, G. *et al.* CD133 antigen expression in ovarian cancer. *BMC Cancer* **9**, 221 (2009).
42. Curley, M. D. *et al.* CD133 expression defines a tumor initiating cell population in primary human ovarian cancer. *Stem Cells* **27**, 2875–2883 (2009).

43. Silva, I. A. *et al.* Aldehyde dehydrogenase in combination with CD133 defines angiogenic ovarian cancer stem cells that portend poor patient survival. *Cancer Res* **71**, 3991–4001 (2011).
44. Munro, M. J. *et al.* Cancer stem cell subpopulations in primary colon adenocarcinoma. *PLoS One* **14**, e0221963 (2019).
45. Tang, B. *et al.* A Flexible Reporter System for Direct Observation and Isolation of Cancer Stem Cells. *Stem Cell Reports* **4**, 155–169 (2014).
46. Boyle, K. E., Boger, D. L., Wroe, A. & Vazquez, M. Duocarmycin SA, a potent antitumor antibiotic, sensitizes glioblastoma cells to proton radiation. *Bioorg Med Chem Lett* **28**, 2688–2692 (2018).
47. Pariset, E. *et al.* DNA Damage Baseline Predicts Resilience to Space Radiation and Radiotherapy. *Cell Rep* **33**, 108434 (2020).
48. Walcher, L. *et al.* Cancer Stem Cells-Origins and Biomarkers: Perspectives for Targeted Personalized Therapies. *Front Immunol* **11**, 1280 (2020).
49. Sun, J.-H., Luo, Q., Liu, L.-L. & Song, G.-B. Liver cancer stem cell markers: Progression and therapeutic implications. *World J Gastroenterol* **22**, 3547–3557 (2016).
50. Resveratrol Suppresses Epithelial-Mesenchymal Transition in GBM by Regulating Smad-Dependent Signaling. https://www.hindawi.com/journals/bmri/2019/1321973/.